Ultrafast Bond Softening in Bismuth: Mapping a Solid's Interatomic Potential with X-rays

Submitted to Science

Stanford Linear Accelerator Center, Stanford University, Stanford, CA 94309

D. M. Fritz,[1,2]* D. A. Reis,[1,2] B. Adams,[3] R. A. Akre,[4] J. Arthur,[5] C. Blome,[6]
P. H. Bucksbaum,[2,4,7] A. L. Cavalieri,[8] S. Engemann,[5] S. Fahy,[9] R. W. Falcone,[10]
P. H. Fuoss,[11] K. J. Gaffney,[5] M. J. George,[5] J. Hajdu,[12] M. P. Hertlein,[13]
P. B. Hillyard,[14] M. Horn-von Hoegen,[15] M. Kammler,[15] J. Kaspar,[14]
R. Kienberger,[8] P. Krejcik,[4] S. H. Lee,[1] A. M. Lindenberg,[5] B. McFarland,[7]
D. Meyer,[15] T. Montagne,[4] É. D. Murray,[9] A. J. Nelson,[17] M. Nicoul,[15]
R. Pahl[18], J. Rudati,[3] H. Schlarb,[6] D. P. Siddons,[19] K. Sokolowski-Tinten,[15]
Th. Tschentscher,[6] D. von der Linde,[15] J. B. Hastings[5]

[1]FOCUS Center, Departments of Physics and Applied Physics Program

University of Michigan, Ann Arbor, MI 48109, USA

[2]PULSE Center, Stanford Linear Accelerator Center, Menlo Park, CA 94025, USA

[3]Advanced Photon Source, Argonne National Laboratory, Argonne, IL 60439, USA

[4]Stanford Linear Accelerator Center, Menlo Park, CA 94025, USA

[5]Stanford Synchrotron Radiation Laboratory/SLAC, Menlo Park, CA 94025, USA

[6]Deutsches Elektronen-Synchrotron DESY, Notkestrasse 85, 22607 Hamburg, Germany

[7]Departments of Physics and Applied Physics, Stanford University, Stanford, CA 94305, USA

[8]Max-Planck-Institute of Quantum Optics, Hans-Kopfermann-Strasse 1, D-85748 Garching, Germany

[9]Department of Physics and Tyndall National Institute, University College, Cork, Ireland

[10]Department of Physics, University of California, Berkeley, CA 94720, USA

[11]Materials Science Division, Argonne National Laboratory, Argonne, IL 60439, USA

[12]Department of Cell and Molecular Biology, Biomedical Centre, Uppsala University, SE-75124 Uppsala, Sweden

[13]Lawrence Berkeley National Laboratory, Berkeley, CA 94720, USA

[14]Department of Chemistry, Stanford University, Stanford, CA 94305, USA

[15]Institut für Experimentelle Physik, Universität Duisburg-Essen, 47057 Duisburg, Germany

[16]Institut für Halbleitertechnologie, Universität Hannover

[17]Lawrence Livermore National Laboratory, Livermore, CA 94550, USA

[18]Consortium for Advanced Radiation Sources, The University of Chicago, Chicago, IL 60637, USA

[19]National Synchrotron Light Source, Brookhaven National Laboratory, Upton, NY 11973, USA

*To whom correspondence should be addressed; E-mail: dmfritz@slac.stanford.edu.

Intense femtosecond laser excitation can produce transient states of matter that would otherwise be unaccessible to laboratory investigation. At high excitation densities, the interatomic forces that bind solids and determine many of their properties can be significantly altered. Here we present the detailed mapping of the carrier density-dependent interatomic potential of bismuth approaching a solid-solid phase transition. Our experiments combine stroboscopic techniques using a high brightness linear electron accelerator based X-ray source with pulse-by-pulse timing reconstruction for femtosecond resolution, allowing quantitative characterization of the interatomic potential energy surface of the highly excited solid.

The availability of bright sources of ultrafast hard x-rays, such as future free-electron lasers, opens up the possibility to follow atomic motion stroboscopically with the picometer spatial and femtosecond temporal resolution required to capture the fastest atomic vibrations and the making and breaking of chemical bonds (*1*). However, the inability to precisely time the x-ray probe can lead to significant reduction in temporal resolution. Recently, the use of single-shot determination of the x-ray arrival time as a means of random sampling has been demonstrated to circumvent this problem (*2*). Using this technique, we report on femtosecond laser pump x-ray-probe experiments that elucidate the role that carrier-induced bond-softening and anharmonicity play in the high-amplitude phonon dynamics of photoexcited bismuth.

The valence electrons and ionic cores (nucleus and core electrons) that comprise a crystalline solid, in general, can be considered as distinct components that couple through the electron-lattice interaction. In bismuth, as well as antimony and tellurium, the electron lattice interaction is strong and the lattice configuration is sensitive to the population distribution of electrons within the conduction bands. In these materials, femtosecond photoexcitation of charge carriers drives the symmetric zone center A_{1g} coherent optical phonon mode (*3–5*). The

vibrational excitation is generally believed to be displacive: the population redistribution of valence electrons alters the potential energy surface of the lattice and gives rise to a restoring force that drives coherent atomic motion. The dynamics of this mode are determined by the curvature and minima location of the altered potential energy surface (quasi-equilibrium coordinate). Knowledge of these parameters is required for predictive models of the non-equilibrium behavior. Similar electronically excited energy surfaces are relevant in understanding a range of important processes in nature, from photo-catalysis to non-equilibrium charge transport in nanojunctions.

Experimentally, the A_{1g} vibrational mode has been monitored indirectly by measuring time-dependent optical reflectivity (*3, 6–10*), and directly by time-resolved x-ray diffraction measurements (*11*). However, with the latter technique, low x-ray flux prevented carrier dependent studies of the interatomic potential. Recent observations in bismuth and tellurium reveal that the vibrational frequency is not constant: it red-shifts from the equilibrium value under high intensity excitation, indicating a softened phonon mode (*7, 9–12*). Subsequent to the initial softening, the oscillation frequency blue-shifts back towards the equilibrium value as the oscillation amplitude and carrier density decay (*9, 10*). The mechanism responsible for this time-dependent vibrational frequency shift, or chirp, has been controversial. Hase *et al.* concluded that the chirp was due to an amplitude-dependent frequency caused by anharmonicity of the interatomic potential (*9*). Fahy and Reis suggested an alternate explanation based on electronic softening of the potential and the subsequent dynamics of the photoexcited carriers (*13*). Optical coherent control experiments in which the phonon amplitude was varied at fixed electronic excitation demonstrated that the observed phonon frequency is dominated by electronic effects and that anharmonicity in the interatomic potential plays a negligible role, a finding that was supported by ab-initio constrained density functional theory (DFT) calculations (*10*). However, as optical reflectivity does not measure atomic positions, the location of the potential energy minimum

and the amplitude of the phonon-driven atomic displacement could not be determined.

Here we use femtosecond x-ray diffraction to elucidate the dynamics of the high-amplitude phonons by direct measurement of the atomic positions within the unit cell. The knowledge of the time evolution of the atomic positions enables the determination of the quasi-equilibrium coordinate and curvature of the interatomic potential, and the comparison of these parameters to previous DFT calculations. The potential well shifts and softens with increasing carrier density, corresponding to a highly-excited solid in which a significant fraction of the total valence electrons are promoted to the conduction bands.

The room temperature structure of bismuth is rhombohedral A7 with two atoms per unit cell. The lattice geometry is a Peierls distortion of simple cubic, with alternating atoms spaced non-equidistantly along the body diagonal or trigonal axis (Fig. 2). Thus, there exists a double well interatomic potential with normalized equilibrium coordinate at $x = 0.5 \pm \delta$ (in units of the hexagonal unit cell length, $c =$1.18 nm). The A_{1g} mode consists of an oscillation of the two basis atoms along the trigonal direction, and thus x is also the phonon coordinate. δ is a measure of the Peierls distortion, i.e., the deviation of each potential energy minimum from the symmetric $x = 0.5$ point. The quasi-equilibrium coordinate and shape of the well constraining the atoms along the trigonal direction are sensitive to excitation of carriers from the valence band to the conduction band (*10*).

A 50 nm thick bismuth film grown by molecular beam epitaxy with a (111) surface orientation (*14*) was excited at room temperature by near-infrared pulses (70 fs FWHM) propagating from a Ti:sapphire laser system in a direction co-linear with the x-rays. The x-ray pulses (10^6 photons at 9 keV , 0.24 mm^2 area, 100 fs duration) were generated from the Sub-Picosecond Pulse Source (SPPS) at the Stanford Linear Accelerator Center (SLAC). The (111) x-ray Bragg reflection was observed for absorbed excitation fluences between 0.3 and 3.0 mJ/cm^2 per pulse at a 10 Hz repetition rate (*15*). We note that at 1.5 mJ/cm^2, enough energy is deposited to even-

tually raise the temperature of the entire film to the melting point, although at least 4.1 mJ/cm^2 is required to provide the additional latent heat for thermal melting. It is in this high fluence regime that ultrafast excitation of carriers generates large amplitude coherent phonons with a significantly lowered frequency.

During the first few picoseconds after excitation, it appears that the absorbed energy is stored almost entirely in the electronic degrees of freedom and the mechanical vibration associated with the A_{1g} mode. In this time, the volume of the unit cell remains fixed and the lattice remains at room temperature. On the time scale of a ~ 20 picoseconds, significant uniaxial strain is observed as a shift in the Bragg angle. Thus the observed changes in the diffraction efficiency at these early times (Fig 1.) are due to structural changes within the unit cell of the crystal. The structure factor for the (hkl) Bragg reflection is a function of the phonon coordinate

$$F = 2f_{Bi} \cos\left[\pi(h + k + l)x\right],$$

where f_{Bi} is the atomic scattering factor for bismuth. In the limit of a thin film and constant temperature, the x-ray diffraction efficiency for the (111) reflection is a direct measure of the atomic displacement along the trigonal direction

$$I(t)/I(0) = \cos^2\left[3\pi x(t)\right]/\cos^2\left[3\pi x(0)\right].$$

A large transient decrease in diffraction efficiency occurs upon the arrival of the excitation pulse ($t = 0$), and is followed by damped oscillations superimposed upon a recovery. In the high-symmetry, non-Peierls distorted state, $x = 0.5$ and the (111) reflection is forbidden by symmetry. Thus, the transient decrease is attributed to a sudden shift in the minima location of the potential energy surface (towards $x = 0.5$) in the excited electronic state, leading to atomic oscillations about the shifted equilibrium. Measurements of the (222) reflection, which increases in intensity for the higher-symmetry arrangement, confirm this attribution. A similar behavior was observed by Sokolowski-Titen *et al.* (*11*). The quasi-equilibrium coordinate is

6

then measured directly from the magnitude of the transient decrease seen in the (111) data (coordinate the oscillations are occurring about). The subsequent increase is ascribed to carrier relaxation through diffusion and recombination, which eventually restores the potential energy surface to its equilibrium shape at excitation levels below the damage threshold.

The oscillatory part of the diffraction signal, corresponding to the coherent optical phonon mode, was fit to a decaying sinusoid with fixed frequency and varying initial phase. Because the phonon frequency is chirped, the frequency obtained from the fit represents the average phonon frequency over the fitting interval (~ 0.5 to 1.5 ps). The measured value, ranging from 2.84 to 2.31 THz, is red-shifted relative to that observed in CW Raman scattering experiments (2.93 THz) (*8*). Similar softening has been measured in optical experiments (*7, 9, 10*).

The inset of Fig. 1 displays the dependence of phonon frequency on the quasi-equilibrium coordinate (measured over the same time interval as the phonon frequency). Our results also represent average values over the sample depth for both frequency and quasi-equilibrium coordinate, as the x-ray penetration depth is much larger than the film thickness. In the absence of photoexcitation, the accepted values of the frequency and equilibrium location at room temperature are 2.93 THz and $x = 0.46719$ (*10, 16–18*). Note that at a measured quasi-equilibrium coordinate of $x = 0.4729 \pm 0.0001$, the well is shifted by 6.7 picometers and the interatomic forces are softened by 35% ($\sim 20\%$ decrease in the phonon frequency). The results are compared with the constrained DFT calculation of Murray *et al.* (*10*) (dotted line). These first-principles calculations assumed production of a single electron-hole pair per absorbed photon and rapid thermalization of the electrons and holes by intraband scattering, followed by electron-hole recombination on a longer time scale. Therefore, the electron and hole distributions are approximated as independent Fermi-Dirac distributions with separate chemical potentials such that the average energy of each pair is equal to the photon energy. Despite these approximations, the excellent agreement with experimental results here demonstrates the ability of DFT to quantita-

7

tively predict the essential excited state features (quasi-equilibrium coordinate and frequency) of this system.

Under the same assumption of a single electron hole pair produced per absorbed photon, we separately compare the measured quasi-equilibrium coordinate as a function of carrier density to the DFT predictions (Fig. 2). The calculated double well potential with the quasi-equilibrium coordinate is indicated by the dotted line (for illustrative purposes we arbitrarily chose the $x < 0.5$ well). The curving of the dotted line towards $x = 0.5$ shows that increasing carrier density reduces the Peierls distortion. The shift in equilibrium coordinate was measured for carrier densities spanning 0.18% to 1.8% of the total valence electrons, averaged over the 50 nm film. A transient displacement of 11 picometers was observed for the highest carrier density and corresponds to 2.0% of the equilibrium interatomic separation along the trigonal axis. Note that this value is not the same as the change in nearest neighbor distance, which is approximately a factor of two smaller. Higher excitation levels led to irreversible damage to the material which was evident as an overall decrease in the diffraction efficiency for the unexcited crystal.

The calculations suggest that upon excitation of approximately 2.5% of the valence electrons, bismuth undergoes a structural phase transition to a higher symmetry state, whereas at approximately 2% excitation the barrier between the wells is lowered sufficiently for the atoms to move in both wells (*19*). It is unclear, for an initial room temperature lattice, whether this level of excitation density can be achieved without subsequent thermal melting of the material (or what role formation of domains plays in the melting transition). We also note that at these excitation levels there is no evidence, either experimentally or in the DFT results, of a nonthermal melting transition such as that found in tetrahedrally bonded semiconductors (*20–24*).

In addition to the quasi-equilibrium coordinate, we also extract the carrier density dependent curvature of the potential well from the measured frequency of the A_{1g} mode assuming a harmonic potential (solid black curves in Fig. 3). The extent of the curves represents the max-

imum range of motion of the ions that occurs in the limit of a purely displacive excitation. A comparison of these results with the potential calculated by DFT (dotted lines, corresponding to fixed density cross-sections of the surface shown in Fig. 2) shows that for carrier densities as high as 1%, the atoms are well described as moving in a purely harmonic potential. At the highest carrier density in which we could extract a phonon frequency from the data, the calculations predict only a slight deviation from a harmonic potential. This result is reinforced by the excellent agreement between the measured and calculated frequency (which includes the anhamonic terms) as a function of carrier density (Fig. 3 inset). Thus although anharmonicity must be present at some level, electronic softening by far dominates the determination of the phonon frequency at the high excitation densities in this and former experiments.

The present study provides one example of the potential applications and scientific applications of time-resolved structural measurements on both the atomic length and atomic time scale. Two significant technical advances enabled this study: the generation of high x-ray photon flux in a temporally short pulse from a linear accelerator source, and the ability to measure the relative x-ray and laser pulse arrival times. Standard stroboscopic measurements in the sub-picosecond time regime derive the excitation pulse and probe pulse from the same ultrafast source with the pump-probe relative delay determined by the optical path length difference. This setup ensures synchronization between pump and probe and realizes the temporal limit set by the probe pulse duration. In experiments where the pump and probe are derived from separate sources, such as the study reported in this manuscript, synchronization is not inherent and must be actively attained. To achieve temporal resolution of the order of x-ray pulse duration, it is necessary to either synchronize the two sources to a fraction of the probe pulse duration or to measure the relative arrival time on a shot-by-shot basis. Due to sources of jitter in the linear electron accelerator that cannot be mitigated, particularly electron bunch energy fluctuations, synchronization to the level of the x-ray pulse duration is not achievable and a relative time of

9

arrival measurement is essential for experiments that require multi-shot data acquisition.

Temporal resolution of ~100 femtoseconds, required to observe coherent phonon motion in bismuth, was achieved by measuring the relative arrival time of the electron bunches using electro-optic sampling (EOS) (*2*). Laser pulses, split from the same source used to photoexcite the bismuth film, were transported via optical fiber to the electron beam (*25*). The measured electro-optic signal from the electron bunch was as short as 170 fs FWHM, and the centroid of this feature was determined to sub-20 fs precision and used as a time stamp for the relative time of arrival. The temporal jitter between the pump and probe provided random sampling of time points. X-ray data obtained from diffraction measurements were sorted into 40 fs time bins according to the time of arrival measured through EOS (see Fig. 4). Data within a time bin were averaged together to increase the signal-to-noise ratio.

References and Notes

1. R. F. Service, *Science* **298**, 1356 (2002).

2. A. L. Cavalieri, *et al.*, *Phys. Rev. Lett.* **94**, 114801 (2005).

3. T. K. Cheng, *et al.*, *Appl. Phys. Lett.* **59**, 1923 (1991).

4. H. J. Zeiger, *et al.*, *Phys. Rev. B.* **45**, 768 (1992).

5. T. Stevens, J. Kuhl, R. Merlin, *Phys. Rev. B* **65**, 144304 (2002).

6. T. K. Cheng, *et al.*, *Appl. Phys. Lett.* **57**, 1004 (1990).

7. M. F. DeCamp, D. A. Reis, P. H. Bucksbaum, R. Merlin, *Phys. Rev. B.* **64**, 092301 (2001).

8. M. Hase, K. Mizoguchi, H. Harima, S. Nakashima, K. Sakai, *Phys. Rev. B.* **58**, 5448 (1998).

9. M. Hase, M. Kitajima, S. Nakashima, K. Mizoguchi, *Phys. Rev. Lett.* **88**, 67401 (2002).

10. E. D. Murray, D. M. Fritz, J. K. Wahlstrand, S. Fahy, D. A. Reis, *Phys. Rev. B* **72**, 060301(R) (2005).

11. K. Sokolowski-Tinten, *et al.*, *Nature* **422**, 287 (2003).

12. S. Hunsche, K. Wienecke, T. Dekorsy, H. Kurz, *Phys. Rev. Lett.* **75**, 1815 (1995).

13. S. Fahy, D. A. Reis, *Phys. Rev. Lett.* **93**, 109701 (2004).

14. M. Kammler, M. Horn-von Hoegen, *Surf. Sci.* **576**, 56 (2005).

15. The absorbed laser energy was measured by subtracting the reflected laser energy from the incident energy. The absorbed fluence was then computed with knowledge of the laser intensity profile. This measurement takes into account the optical properties of bismuth for the particular incidence angle and laser polarization used. Only the incident fluence was stated in many of the cited references and therefore the optical properties of bismuth must be taken into account before directly comparing the results.

16. P. Fischer, I. Sosnowska, M. Szymanski, *J. Phys. C: Solid State Phys.* **11**, 1043 (1978).

17. X. Gonze, J.-P. Michenaud, J.-P. Vigneron, *Phys. Rev. B.* **41**, 11827 (1990).

18. An experimental ambuiguity regarding the room temperature equilibrium position exists: A measurement of 0.4668 was cited in (14) and 0.46814 was cited in (15). The chosen value of 0.46719, the equilibrium value determined by DFT, was used to best compare experimental results to DFT calculations.

19. Note that this phase transition is distinct from the Bi I-II transition that occurs at 25.3 kbar of hydrostatic pressure (P.W. Bridgman, *Proc. Am. Acad. Arts Sci.* **74**, 438 (1942)).

20. R. Biswas, V. Ambegaokar, *Phys. Rev. B* **26**, 1980 (1982).

21. C. V. Shank, R. Yen, C. Hirlimann, *Phys. Rev. Lett.* **50**, 454 (1983).

22. P. Stampfli, K. H. Bennemann, *Phys. Rev. B* **49**, 7299 (1994).

23. A. M. Lindenberg, *et al.*, *Science* **308**, 392 (2005).

24. V. Recoules, J. Clérouin, G. Zérah, P. M. Anglade, S. Mazevet, *Phys. Rev. Lett.* **96**, 055503 (2006).

25. S. H. Lee, A. L. Cavalieri, D. M. Fritz, M. Myaing, D. A. Reis, *Opt. Lett.* **29**, 2602 (2004).

Fig. 1. Bismuth (111) X-ray diffraction efficiency as a function of time delay between the optical excitation pulse and X-ray probe for excitation fluences of 0.7 (green), 1.2 (red), 1.7 (blue) and 2.3 mJ/cm^2 (grey). The zero delay point was set at the half maximum of the intial transient drop. The inset displays the optical phonon frequency as a function of the normalized atomic equilibrium position along the body diagonal of the unit cell x as measured via x-ray diffraction. The dotted curve represents the theoretical prediction obtained from DFT calculations of the excited state potential energy surface (*10*).

Fig. 2. Interatomic quasi-equilibrium position as a function of the percentage of valence electrons promoted into the conduction band. The red circles represent experimental results while the dotted line depicts the potential minimum obtained from the DFT potential landscape. The adjusted potential energy surface obtained from DFT is overlayed in false color representation (*10*). The bismuth unit cell is displayed in the upper right quadrant. The red bar represents the body diagonal length c and the yellow bar represents the basis atom coordinate xc.

Fig. 3. Interatomic potential curvature as a function of carrier density. Solid lines represent the region of the interatomic potential sampled by the atoms under complete displacive excitation. The curvature was derived from the measured phonon frequency assuming pure harmonic motion. Dotted lines are cross-sections of the DFT interatomic potential surface displayed in Fig. 2 for fixed carrier densities. The vertical scale is adjusted for clarity and the potential energy is displayed relative to the minimum of the unexcited structure. The inset displays the phonon frequency as a function of carrier density. The dotted line shows A_{1g} frequencies from DFT frozen phonon calculations. The starred point is the equilibrium Raman value of the .

Fig. 4. a) One-hundred consecutive electro-optic signals. The centroid of the signal is used to determine the relative electron bunch-laser pulse arrival time. A total temporal jitter of 2 ps is observed. b) Histograms of the measured electron bunch arrival times are displayed on the right for N = 10, 100, and 1000 shots. The corresponding x-ray data, arranged sequential

by determined arrival time by electro-optic sampling, are shown on the left. A movie of data acquisition in real time is included as supporting online material.
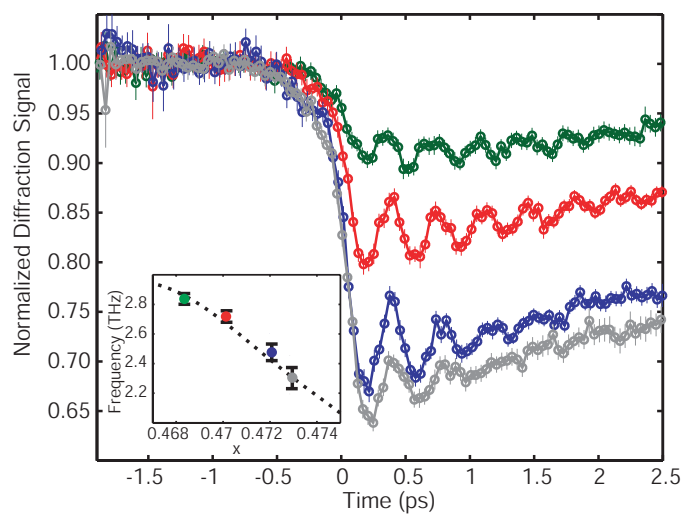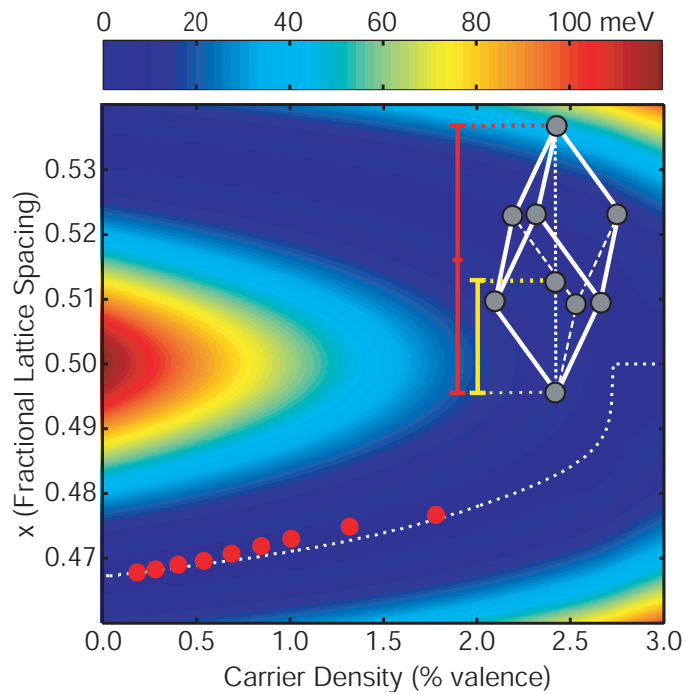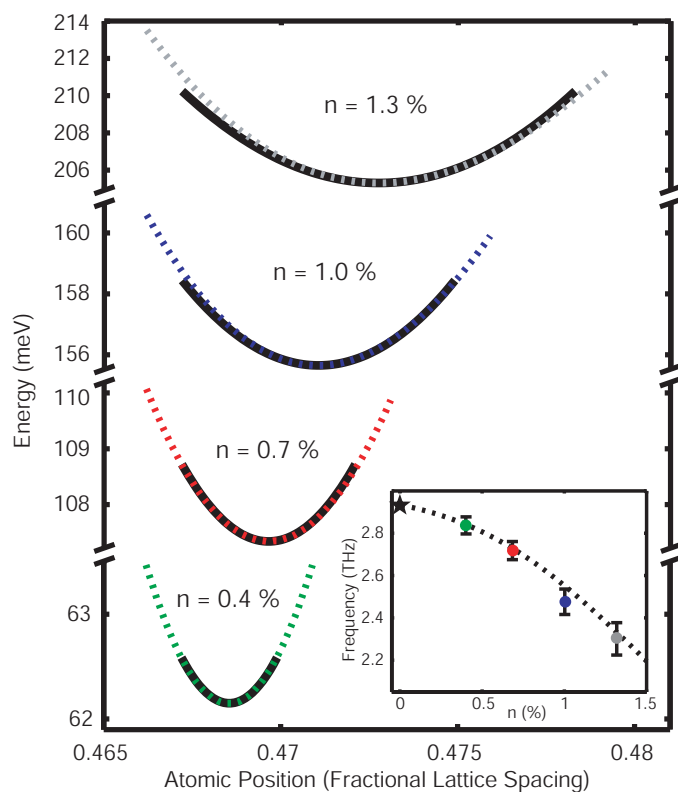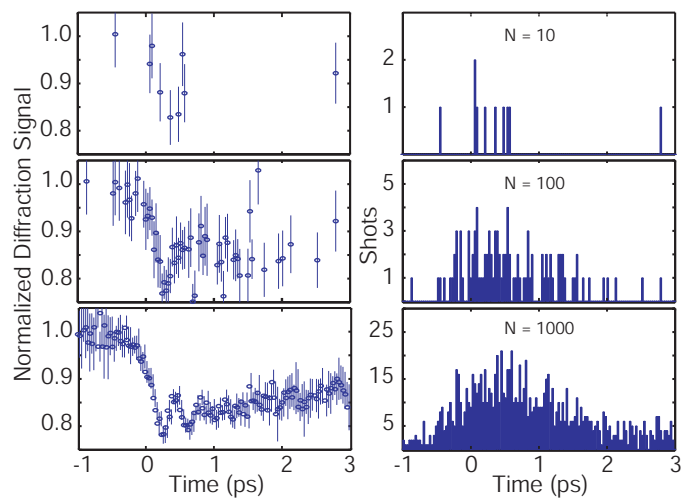
Figure 1:

Figure 2:

15

Figure 3:

Figure 4: